RbCs bands observation and interpretation

R. BEUC[1]
M. MOVRE[1,✉]
B. HORVATIĆ[1]
M. ČOPOR[1]
S. VDOVIĆ[1]
A. NEVSESYAN[2]
T. VARZHAPETYAN[2]
D. SARKISYAN[2]
G. PICHLER[1]

[1] Institute of Physics, Bijenička cesta 46, P.O. Box 304, 10001 Zagreb, Croatia
[2] Institute for Physical Research, NAS of Armenia, Ashtarak-2 378410, Armenia

ABSTRACT We calculated the approximate form of absorption bands of RbCs molecules in the 450–1000 nm wavelength range. The manifold of potential curves for the Hund's coupling case a was used to predict the absorption spectra assuming constant transition dipole moments, which can serve as a first approximation for the comparison with experimental results and their interpretation. Any substantial departure of an observed spectrum from the predicted one would point to the need of more complex calculations comprising transition-dipole-moment functions and spin–orbit interaction. Comparison with RbCs absorption bands from hot vapor is discussed. The band at 717 nm is identified as the $1^1\Sigma^+ \to 1^1\Pi$ transition (B–X band) and the diffuse band at 563 nm as the $1^1\Sigma^+ \to 3^1\Pi$ transition.

1 Introduction

Knowledge of theoretical spectra of atoms and molecules is very useful in spectroscopic analysis. Theoretical analysis of the emission spectrum of a mixture of alkali vapors may be of use in designing efficient light sources which have a "pleasant", sun-like spectral distribution. A quick method of evaluation of optical spectra can be used for the analysis of processes in the course of arc ignition and burning in alkali high-pressure arc lamps. This could provide some useful hints for optimization of such light sources [1, 2]. In addition to this, energy conversion with a heavy-alkali-mixture thermionic device may be modeled by the prediction of the broad-band absorption spectrum [3]. Absorption spectroscopy applied to heavier alkali-metal dimers yields dense, unresolvable spectra. In the gas phase the triplet transitions of alkali dimers are usually observed in the form of diffuse and satellite bands, because the lowest $1^3\Sigma_u^+$ electronic state is negligibly populated at thermal energies [4, 5].

RbCs is the heaviest heteronuclear alkali molecule and is of considerable interest for several applications. For example, the RbCs molecule is considered a potential candidate for the formation of Bose–Einstein condensates [6] and ultracold

heteronuclear molecules [7], since both the cold Rb and Cs atoms can be feasibly prepared by diode lasers. It is characterized by a large spin–orbit interaction stemming from both the rubidium and cesium atoms. It also has an appreciable permanent electric dipole moment and thus could be used in current methods of molecular cooling and trapping [8–10]. It has been suggested that the Stark effect in polar alkali-metal dimers could be used as a means to create qubits of a quantum computer [11]. In addition, RbCs can be formed on the surface of a nano-size helium cluster which, as a finite-size cryostat, helps in driving the molecule into the lowest vibrational state of the lowest triplet or singlet electronic states. Also, due to the dynamics of formation of dimers on cold He in the experimental preparation, the ratio of (strongly-bound) singlet to (weakly-bound) triplet dimer states is drastically reduced with respect to its gas-phase value of $1/3$. This facilitates direct photon absorption access to the manifold of the dimers excited triplet states that are negligibly populated and hence poorly detectable even at thermal energies.

In principle it is possible to predict some of the RbCs absorption bands that could be detected in experiments. However, not all necessary transition dipole moments are known at present [12] and furthermore, the standard accuracy of high-quality ab initio calculations is only of the order of $100\,\mathrm{cm}^{-1}$ for the calculated electronic transition energies T_e. Therefore, much additional theoretical work is needed in addition to new spectroscopic measurements.

In the present work we calculate the absorption spectra of the RbCs dimer. We also present the absorption measurements on an Rb-Cs mixture in an all-sapphire cell with Brewster windows, from which we extract detailed shapes of diffuse bands in the green-yellow spectral region. The approximate form of the predicted absorption bands obtained using the rather crude assumption of constant transition dipole moments, combined with the limited knowledge of more detailed spectroscopic data leads us to the conclusion that the band at 717 nm is due to the $1^1\Sigma^+ \to 1^1\Pi$ transition (B–X band) and that the diffuse band at 563 nm should be ascribed to the $1^1\Sigma^+ \to 3^1\Pi$ transition.

2 Experiment

We carried out a series of absorption measurements in a very dense vapor of an Rb-Cs mixture. In Fig. 1a and b

✉ Fax: +385 1 469 88 89, E-mail: movre@ifs.hr
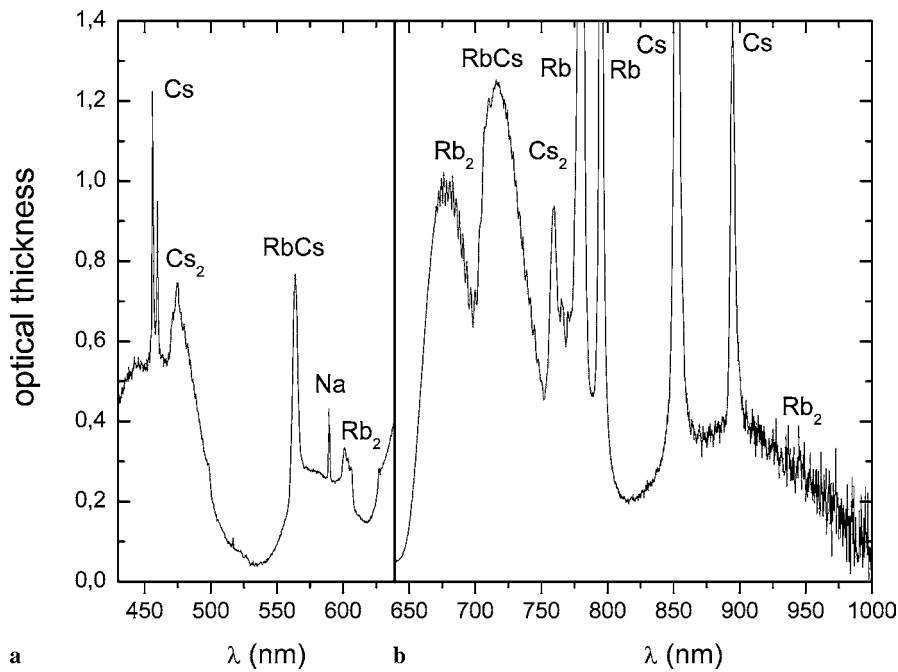
FIGURE 1 Absorption spectrum of a rubidium-cesium mixture in an all-sapphire cell (30 mm in length), obtained with a high-resolution scanning monochromator at temperatures, (**a**) 757 (660) K and (**b**) 641 (570) K. The numbers in parentheses denote the reservoir temperature

we present the optical thickness derived from a white-light transmission spectrum obtained in an all-sapphire cell (30 mm in length) in two spectral regions, each for different alkali vapor temperatures (a) 757 (660) K and (b) 641 (570) K, with the numbers in parentheses giving the reservoir temperature. These temperatures determine the Rb and Cs partial vapor pressures inside the all-sapphire cell. The windows of the cell were kept at higher temperatures in order to prevent alkali deposition. The absorption spectrum of the rubidium-cesium mixture was resolved with a high-resolution scanning monochromator.

The recorded spectrum is a superposition of individual Rb_2, Cs_2 and RbCs bands. In Fig. 2a, on the left, one can see a peak lying close to the Cs $7P$ doublet (455,5/459,3 nm). It is actually a superposition of three contributions, comprising the Cs_2 $E-X$ band centered at 480 nm [13, 14], the Rb_2 $D-X$ band peaking at 475 nm [13, 15] and the RbCs $1^1\Sigma^+ \rightarrow 4^1\Pi$ band [10]. The Rb_2 $1^3\Sigma_u^+ \rightarrow 2^3\Pi_g$ diffuse band [15] lies next to the Na $3P$ unresolved doublet at 590 nm, but there is only one feature, visible at 563 nm, which could be unambiguously attributed only to an RbCs transition. The main features shown in Fig. 1b are the Rb_2 and Cs_2 $B-X$ bands [13], while the band lying at 717 nm between them could be recognized as the RbCs $B-X$ band (see below). Towards the larger wavelengths one can see the collisionally-broadened Rb D lines as well as Cs D lines, the latter sitting on the Rb_2 $A-X$ band [13].

3   Theoretical simulations

The particular contributions to the absorption coefficient from hot vapor were calculated applying the semiclassical approach described in [16]. In the simple quasistatic approximation, the classical absorption spectra generally agree with the overall quantum mechanical band shapes, except for nearly periodic band structures and nonclassical behavior at the satellite positions. The present refined treatment of the spectra, based on the uniform Airy approximation, avoids singularities pertinent to the quasistatic line shapes and takes into account interferences among the contributions of various Condon points. The potentials of the excited states relevant for singlet and triplet transitions [17] are shown in Fig. 2. Zero energy corresponds to the $Rb(5\,^2S) + Cs(6\,^2S)$ asymptote. In addition, the corresponding difference potentials are
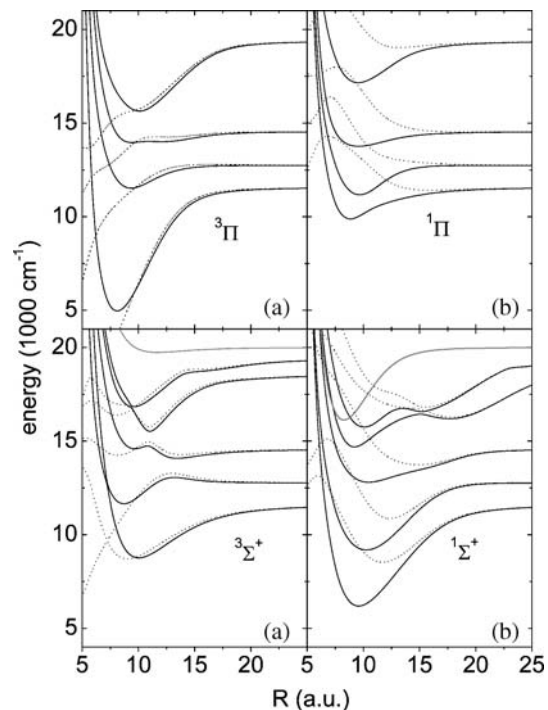
FIGURE 2 Potential curves of the excited states (*solid lines*) from [17]: (**a**) $^3\Pi$, (**b**) $^1\Pi$, (**c**) $^3\Sigma^+$, (**d**) $^1\Sigma^+$. The corresponding difference potentials (*dotted lines*) are also shown. Zero energy is taken to be the $Rb(5\,^2S) + Cs(6\,^2S)$ asymptote

indicated by dotted lines. The extrema of the difference potentials often correspond to the satellite bands in the observed spectra.

The practical aim of theoretical simulations of the bands is identification of the experimentally observed ones, i.e., their attribution to particular radiative transitions among the RbCs dimer states. These simulations have additional value to applications, as they give predictions that can facilitate the search for bands suitable for particular technological purposes, e.g., such as would enrich the spectrum of alkali-vapor lamps.

It turns out that this can be achieved with quite modest means, i.e., that the rather crude model we use (Hund's coupling case a, constant transition dipole moments, no spin–orbit effects) has proved quite efficient in this respect, as it sufficiently obtains recognizable and fairly accurate theoretical simulations of the RbCs absorption bands.

Figure 3 shows particular contributions to the reduced absorption coefficient calculated semiclassically, as described in [16], assuming all molecular oscillator strengths are asymptotically ($R \rightarrow \infty$) equal to unity. This implies that the calculated contributions corresponding to different transi-

tions are not up to scale – in our theoretical simulations we aim at the positions and shapes of the bands, as accurate as possible within the above-specified limitations, but not at their absolute intensities. All simulations were made for a single temperature $T = 720$ K, intermediate between the two experimental ones. Note that some of the transitions are asymptotically forbidden (shown by dotted-line curves in Fig. 3), i.e., their oscillator strengths tend asymptotically to zero. The bands lying between the asymptotes are very likely to be observed, since the induced dipole moment will be nonzero at the relevant internuclear distances. However, those peaks that lie on the forbidden asymptotes will not be observable, although predicted by our simplified model.

Figure 3a displays the $1^3\Sigma^+ \rightarrow N^3\Pi$ transitions. (Here and throughout the paper, N labels the states of a given symmetry in the order of increasing energies.) All contributions to the absorption coefficient are found in close proximity to the atomic lines. Such contributions are of minor importance in the present context of finding the (relatively broad) bands that could enrich the spectrum of the mixed alkali-vapor lamps. Figure 3b suggests that the $1^1\Sigma^+ \rightarrow 1^1\Pi$ (B–X band) and $1^1\Sigma^+ \rightarrow 3^1\Pi$ transitions are clearly distinguishable in the spectrum of an Rb-Cs mixture. As already mentioned, the $1^1\Sigma^+ \rightarrow 4^1\Pi$ transition is overlapped by the Cs$_2$ E–X and Rb$_2$ D–X bands. The spectrum of Fig. 3c ($1^3\Sigma^+ \rightarrow N^3\Sigma^+$ transitions) is also found to be confined to the vicinity of the atomic lines, but Fig. 3d shows that some of the displayed $1^1\Sigma^+ \rightarrow N^1\Sigma^+$ transitions could significantly contribute to spectra of the types relevant for the above-mentioned purposes.

Figure 4 displays the details of the $1^1\Sigma^+ \rightarrow 3^1\Pi$ transition from Fig. 3b and compares the semiclassical simulation of the reduced absorption coefficient to an expanded view of the corresponding part of the experimental spectrum of Fig. 1a comprising the diffuse RbCs band at 563 nm. Unlike Fig. 3, the simulation shown here has been calculated for the temperature at which the corresponding experimental results were obtained, $T = 757$ K, in order to facilitate comparison. The semiclassical simulation describes the thermal spectrum quite well, except for a shift of the diffuse band which is due to the imprecision of the ab initio difference potentials used (see Sect. 4).

This band turns out to be due to a singlet transition, $1^1\Sigma^+ \rightarrow 3^1\Pi$, contrary to what one would expect from its appearance (a smooth, structureless peak, typically characteristic of triplet transitions). This is already indicated experimentally by the observed temperature dependence of the band intensity, in contrast to triplet transitions, for which the temperature dependence in absorption is usually negligible. Further support is provided by the decomposition of the predicted spectrum into two components, one due to the bound–bound transitions and the other one to the bound–free ones: it is the latter component that gives the predominant contribution to the RbCs peak. Contributions of the bound–bound transitions are indicated by right-slanted hatching and those of the bound–free transitions by left-slanted hatching. The total absorption coefficient (their sum) is given by the curve with no hatching. Note that where the two contributions become comparable (to the right of the peak), one does observe discrete structure in the experimental curve. Whether this is indeed due
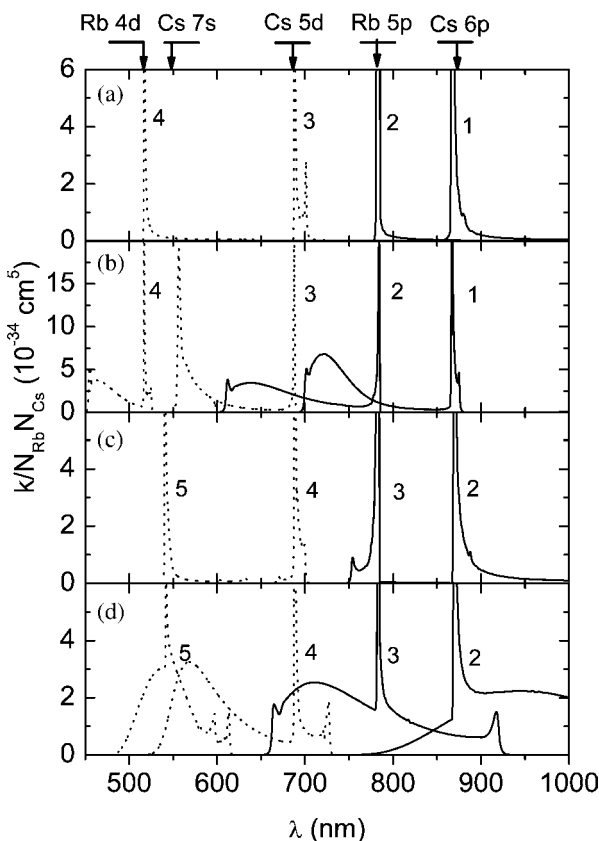
FIGURE 3 Particular contributions to the reduced absorption coefficient from hot ($T = 720$ K) RbCs vapor calculated applying the semiclassical approach described in [16]: (**a**) $1^3\Sigma^+ \rightarrow N^3\Pi$ ($N = 1, 2, 3, 4$), (**b**) $1^1\Sigma^+ \rightarrow N^1\Pi$ ($N = 1, 2, 3, 4$), (**c**) $1^3\Sigma^+ \rightarrow N^3\Sigma^+$ ($N = 2, 3, 4, 5$), (**d**) $1^1\Sigma^+ \rightarrow N^1\Sigma^+$ ($N = 2, 3, 4, 5$). The relevant difference potentials are shown in Fig. 2. *Solid-line curves* denote asymptotically-allowed transitions and *dotted-line curves* denote asymptotically-forbidden ones, respectively. All *sharp bands* that lie on the forbidden asymptotes are artifacts of the assumed constant dipole moments and will not be observable. The *arrows* along the upper edge indicate the positions of the atomic asymptotes
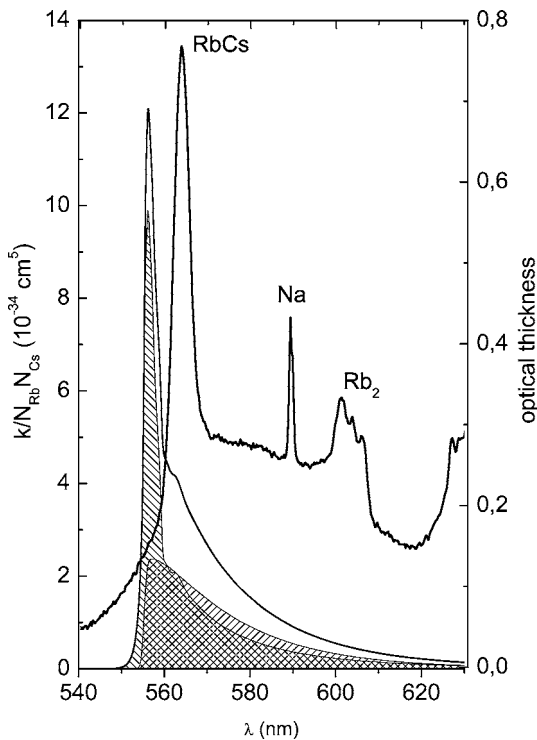
FIGURE 4 The portion of the thermal spectrum between 540 and 630 nm comprising the diffuse RbCs band at 563 nm. Semiclassical simulation of the reduced absorption coefficient due to the RbCs $1^1\Sigma^+ \to 3^1\Pi$ transition is compared to the corresponding part of the experimental spectrum (see Fig. 1a) for the same temperature $T = 757$ K. The predicted spectrum (no hatching) is also decomposed into the bound–bound component (right-slanted hatching) and the bound–free one (left-slanted hatching)

FIGURE 5 The portion of the thermal spectrum between 640 and 790 nm comprising the RbCs $B–X$ band at 717 nm, both measured and calculated for the same temperature, $T = 641$ K. Semiclassical simulation of the reduced absorption coefficient is compared to the corresponding part of the experimental spectrum (see Fig. 1b). The predicted spectrum (no hatching) is also decomposed into the bound–bound component (right-slanted hatching) and the bound–free one (left-slanted hatching)

to the discreteness of the bound–bound contribution, and not just to noise, one can not tell with certainty.

The background intensity can be due to several processes, with the RbCs contribution arising from the $1^1\Sigma^+ \to 4, 5^1\Sigma^+$ transitions (see Fig. 3d).

Figure 5 shows the portion of the thermal spectrum between 640 and 790 nm comprising Rb$_2$, RbCs and Cs$_2$ bands. The semiclassical simulation of the reduced absorption coefficient is compared to the corresponding part of the experimental spectrum of Fig. 1b. As in the previous figure, the simulation was calculated for the relevant experimental temperature, here $T = 641$ K. The band at 717 nm, lying between the Rb$_2$ and Cs$_2$ $B–X$ bands, could be recognized as the RbCs $B–X$ band arising from the $1^1\Sigma^+ \to 1^1\Pi$ transition (see Fig. 3b). Contrary to the results for the diffuse RbCs band at 563 nm, in this case the component due to bound–bound transitions gives the predominant contribution to the RbCs band. This is evident in almost the whole region (except at the very left edge of the band), leading to visible vibrational structure. From the difference in the peak positions of the calculated and the observed RbCs $B–X$ bands we estimated that the shift of the calculated RbCs $1^1\Pi$ potential is not greater than $40\,\mathrm{cm}^{-1}$.

The calculations support our findings that the only observable features in the Rb-Cs mixture are the RbCs $B–X$ band ($1^1\Sigma^+ \to 1^1\Pi$) and the $1^1\Sigma^+ \to 3^1\Pi$ diffuse band sitting on the $1^1\Sigma^+ \to 4^1\Sigma^+$ background. There is nothing visible that could be attributed to any RbCs triplet transition, in contrast to

the KRb case [18]. All the other transitions are masked by the transitions of either the Rb$_2$ or Cs$_2$ absorption bands.

4   Discussion and conclusion

As the positions of the bands depend critically on the precision of the potentials, one may judge the quality of the calculated potential curves by comparing the calculated band positions with the experimental ones. Allouche et al. [17] compared their calculated spectroscopic constants with the existing data from spectroscopic investigations of the RbCs molecule (for more details see [17]). The calculated electronic transition energies T_e were found to be shifted by $+7, +47$, and $-3\,\mathrm{cm}^{-1}$ for 3, 4, and $5^1\Sigma^+$ states, respectively, and by $+82, +214$, and $+137\,\mathrm{cm}^{-1}$ for 2, 3, and $4^1\Pi$ states, respectively. The positions of our predicted absorption bands should be shifted by these same amounts (but in the opposite directions) when compared to future experiments in order to fit the theoretically predicted bands to the experimental data.

In a real experiment, some of the peaks (if sufficiently well-resolved) would exhibit fine-structure splitting due to the spin–orbit effects which are neglected in our present simulations. At this time, we are only interested in gross features and modest resolution, keeping possible applications in designing efficient light sources in mind.

Most of the analysis of the observed spectra has been based on the Hamiltonian model expressed in the Hund's case a basis, treating all other interactions (spin–orbit, rotational ...) as perturbations. As clearly stated by Kotochigova and Tiesinga [12], at short internuclear separations the RbCs po-

tentials are described by the $^{(2S+1)}\Lambda^{\pm}$ Hund's case a labeling and the change from the Hund's case a to the relativistic coupling scheme occurring between 20 a_0 and 30 a_0.

The long-range part of the potential curves is relevant for the formation of the wings of the atomic spectral lines, which is not the subject of the present investigation. Instead, we are interested in the spectral regions between the atomic spectral lines where one expects the (more or less) broader molecular bands. These can be diffuse (triplet free–free transitions or singlet bound–free transitions) or vibrationally resolved, corresponding to the bound–bound transitions.

At short-range internuclear separations, the dipole moment is strongly dependent on R and the intensity of the absorption bands would be modulated by the square of the corresponding transition dipole moments. Here, we took constant values for all spin-allowed transitions determined by our assumption of all molecular oscillator strengths being asymptotically equal to unity.

A full theoretical treatment would be very complex, however, we hope that absorption measurements at high densities will help in ascertaining the most prominent transitions in the RbCs molecule. We also have plans for laser-induced fluorescence experiments, which will contribute to the knowledge about the structure of heteronuclear alkali molecules. This knowledge could then be of use in designing efficient light sources or, for example, could be applied to the spectroscopy of RbCs on helium clusters, which currently seems to be the only means available for the observation of RbCs triplet transitions. From our experiments and semiclassical simulations (see Fig. 4), we could deduce the origin of the observed RbCs diffuse bands [19] previously obtained in the cold molecular beam experiment [20].

The present calculations and experiments at thermal energies form a solid basis from which more precise simulations can be performed, accompanied by appropriate experimental investigations. The inclusion of transition-dipole-moment functions is not expected to change our main conclusions.

However, those functions would greatly improve confidence in the comparison with experimental absorption spectra.

REFERENCES

1 H. Gu, M.E. Muzeroll, J.C. Chamberlain, J. Maya, Plasma Sources Sci. Technol. **10**, 1 (2001)
2 G. Pichler, V. Živčec, R. Beuc, Ž. Mrzljak, T. Ban, H. Skenderović, K. Günther, J. Liu, Physica Scripta T **105**, 98 (2003)
3 B.Y. Moyzhes, T.H. Geballe, J. Phys. D Appl. Phys. **38**, 782 (2005)
4 C.M. Dion, O. Dulieu, D. Comparat, W. de Souza Melo, N. Vanhaecke, P. Pillet, R. Beuc, S. Milošević, G. Pichler, Eur. Phys. J. D **18**, 365 (2002)
5 H. Skenderović, R. Beuc, T. Ban, G. Pichler, Eur. Phys. J. D **19**, 49 (2002)
6 G. Roati, F. Riboli, G. Modugno, M. Inguscio, Phys. Rev. Lett. **89**, 150 403 (2002)
7 J. Sage, S. Sainis, T. Bergeman, D. DeMille, Phys. Rev. Lett. **94**, 203 001 (2005)
8 D. Wang, J. Qi, M.F. Stone, O. Nikolayeva, H. Wang, B. Hattaway, S.D. Gensemer, P.L. Gould, E.E. Eyler, W.C. Stwalley, Phys. Rev. Lett. **93**, 243 005 (2004)
9 M.W. Mancini, G.D. Telles, A.R.L. Caires, V.S. Bagnato, L.G. Marcassa, Phys. Rev. Lett. **92**, 133 203 (2004)
10 A. Zaitsevskii, E.A. Pazyuk, A.V. Stolyarov, I. Docenko, I. Klincare, O. Nikolayeva, M. Auzinsh, M. Tamanis, R. Ferber, Phys. Rev. A **71**, 012 510 (2005)
11 D. DeMille, Phys. Rev. Lett. **88**, 067 901 (2002)
12 S. Kotochigova, E. Tiesinga, J. Chem. Phys. **123**, 174 304 (2005)
13 S. Vdović, D. Sarkisyan, G. Pichler, Opt. Commun. **268**, 58 (2006)
14 C. Amiot, W. Demtröder, C.R. Vidal, J. Chem. Phys. **88**, 5265 (1988)
15 T. Ban, D. Aumiler, R. Beuc, G. Pichler, Eur. Phys. J. D **30**, 57 (2004)
16 R. Beuc, V. Horvatić, J. Phys. B **25**, 1497 (1992)
17 A.R. Allouche, M. Korek, K. Fakherddin, A. Chaalan, M. Dagher, F. Taher, M. Aubert-Frécon, J. Phys. B **33**, 2307 (2000)
18 R. Beuc, M. Movre, T. Ban, G. Pichler, M. Aymar, O. Dulieu, W.E. Ernst, J. Phys. B **39**, S1191 (2006)
19 R. Beuc, M. Movre, B. Horvatić, G. Pichler, Chem. Phys. Lett. **435**, 236 (2007)
20 B. Kim, K. Yoshihara, J. Chem. Phys. **100**, 1849 (1994)